Beta-delayed neutron decay of ^{19}N and ^{20}N

C. S. Sumithrarachchi,* D. W. Anthony, P. A. Lofy,† and D. J. Morrissey
National Superconducting Cyclotron Laboratory, Michigan State University, East Lansing, MI 48824 and Department of Chemistry, Michigan State University, East Lansing, MI 48824
(Dated: July 21, 2006)

The results of the first spectroscopic studies of delayed neutron and gamma emission following the beta decay of ^{19}N and ^{20}N are reported. Nuclides were produced by fragmenting a 80 MeV/A ^{22}Ne beam in a 546 mg/cm^2 thick Be target and separated at high velocities with the A1200 fragment separator. The nuclides were implanted in a thin plastic scintillator at the center of an array of neutron scintillators to determine the neutron time-of-flight spectrum. Two Hyper-pure-Ge detectors were used to observe coincident gamma events. The $\beta-\gamma$, $\beta-n$ and $\beta-n-\gamma$ coincidence spectra were analyzed to obtain the energies of the states populated in ^{18}O, ^{19}O and ^{20}O following the beta decay. Eight new neutron energies with the total neutron emission probability of 41.8(9)%, six gamma transitions among the excited states of ^{19}O, and four gamma transitions among the excited states of ^{18}O were identified in the ^{19}N beta decay. Seven new neutron energies with the total neutron emission probability of 42.9(14)%, ten gamma transitions among the excited states of ^{20}O, and two gamma transitions among the exited states of ^{19}O were observed from the ^{20}N beta decay. The half-lives of 336(3) ms and 136(3) ms were determined for ^{19}N and ^{20}N decays, respectively. The branching ratios of both decays were deduced and compared with USD shell model calculations. The beta decay schemes for ^{19}N and ^{20}N were deduced.

PACS numbers: 23.40.-s, 23.20.Lv, 21.60.Cs, 27.20.+n, 27.30.+t
Keywords: Beta-delayed neutron emission, ^{19}N beta decay, ^{20}N beta decay

I. INTRODUCTION

Beta decay measurements of a nuclide provide information on the quantum structure of the daughter nuclide through decay properties such as half-life, beta-delayed particle and gamma emission probabilities and decay strengths. Knowledge of these properties can be used to test structure models and refine the input parameters in order to accurately predict properties of more exotic nuclides. The systematic studies of these properties also can elucidate new trends of nuclear structure. The nature of interactions between nucleons becomes less certain as the neutron number approaches the neutron dripline, so that more knowledge of light nuclei can lead to a clearer understanding of the nature of nuclear structure of heavy, exotic nuclides. Nucleosynthesis calculations also use the decay properties together with reaction measurements to predict stellar properties.

A systematic study of beta-delayed neutron emission of neutron rich nuclei has been carried out at the National Superconducting Cyclotron Laboratory (NSCL). The decay of neutron rich light nuclei is characterized by large Q-values and as the daughter nucleus is often produced in high lying excited states above the neutron separation energy, the emission of beta-delayed neutrons is likely. Spectroscopic neutron measurements are then necessary in order to establish branching ratios to different final states. This paper contains results on the first study of the beta-delayed neutron spectroscopy of ^{19}N and ^{20}N and compares the results with theoretical predictions. Gamma spectroscopic observations of beta decay to neutron bound states for these decays are also reported. The preliminary work on the decay of ^{19}N was presented in Ref.[1].

The first half-life measurement for beta decay of ^{19}N was reported by Dufour et al. as 320(100) ms [2]. The value was re-measured by the same group and reported as 300(80) ms [3]. Dufour et al. published the first half-life measurement of the beta decay of ^{20}N as 70(40) ms [3]. The beta decay of ^{19}N and ^{20}N were studied by Mueller et al. [4] at GANIL using a 4π neutron detector surrounding a semiconductor telescope. They reported total neutron emission probabilities of 33(+34-11)% and 53(+11-7)% with half-lives of 210(+200-100) ms and 100(+30-20) ms for ^{19}N and ^{20}N, respectively. Samuel et al. measured the half-life of ^{19}N at MSU and reported as 235(32) ms [5]. Reeder et al. [6] measured total neutron emission probabilities for these nuclei as 62.4(26)% and 66.1(50)% with half-lives of 329(19) ms and 142(19) ms, respectively. These values were re-measured and reported at a conference by the same group as 54.6(14)% and 57(3)% for total neutron emission probabilities and 271(8) ms and 130(7) ms for half-lives [7]. Although the reported values agree within the errors, the uncertainties are large for the most of measurements. There are no experimental data available for the neutron energies and their transition probabilities for ^{19}N beta decay. Dufour et al. [2] observed three gamma ray transitions for ^{19}N decay at energies of 96.0, 709.2 and 3137.8 keV with relatively poor statistics. The reported relative intensities were 100(10), 76(21) and 63(21) respectively. The gamma transition at 709.2 keV was assigned later to ^{22}O beta decay by Hubert

*Electronic address: chandana@nscl.msu.edu
†New address:Fifth U.S. Army, CSRD, Fort Sam Houston, Texas, 78234.

et al. [8] and recently by Weissman et al. [9] based on a gamma-gated half-life measurement. This makes the ^{19}N beta decay to bound states unclear and suggests the need for more accurate measurements. The energy levels in the daughter ^{20}O have been studied by LaFrance et al. and Young et al. [10, 11] using the ^{18}O(t,p)^{20}O reaction and some of the levels were also investigated using the ^{18}O(α ,2p)^{20}O and ^{18}O(^{18}O,^{16}O)^{20}O reactions [12]. In-beam gamma ray spectroscopic measurements using a single step fragmentation experiment by Stanoiu et al. [13] derived a level scheme for positive parity states under 6 MeV in ^{20}O and a few negative parity states have been observed above 5600 keV. Recent study of excited states in ^{20}O using the reaction ^{10}Be(^{14}C, α)^{20}O by Wiedeking et al. [14] reports five new states not reported in previous observations. There are no beta-delayed neutron or gamma spectroscopic measurements for ^{20}N decay available up to the present.

A shell model prediction for the beta decay of ^{19}N was performed by Warburton [15] using a USD and a modified MKIII interaction for the allowed and first forbidden beta decays, respectively. The prediction was done in the $(0s)^4(0p)^{12}(2s,1d)^3$ model space assuming that ^{19}N has a ground state spin and parity of $1/2^-$. This calculation predicts 12 states that are fed by the allowed beta decays with branches greater than 1% and three states that are fed by the first forbidden beta decays with branches greater than 0.1%. The half-life was predicted to be 0.54 s with a total neutron emission probability of 87%. The beta decay of ^{19}N and ^{20}N to negative parity states have been recently calculated by Brown [16] using the WBP interaction in *s-p-sd* and *s-p-sd-pf* model spaces, respectively. The predictions show major beta branching of 17% and 25% to the states at $E_2^{1/2^-} = 4678$ and $E_5^{3/2^-} = 6326$ keV, respectively, for ^{19}N beta decay and beta branching of 15.2% and 9.2% to the states at $E_2^{2^-} = 6131$ and $E_2^{3^-} = 8400$ keV, respectively, for ^{20}N beta decay. Thus both theoretical calculations give similar values for allowed branching ratios for ^{19}N beta decay but they are not in good agreement with the experimental values measured by Dufour et al. [2]. The total neutron emission probabilities and half-lives predicted from the same calculations are 85.6% and 289 ms for ^{19}N decay and 71.1% and 118 ms for ^{20}N decay.

II. EXPERIMENT

A. Fragment production

The ^{19}N and ^{20}N beams were produced at the NSCL by fragmentation of a 80 MeV/A ^{22}Ne beam in a 546 mg/cm^2 ^{9}Be target. The projectile fragments were separated by the A1200 separator using the momentum-loss achromat mode; a detailed description of the device and method is given in Ref.[17]. The average purities at implantation of ^{19}N and ^{20}N beams were 99.5(1)% and 98.8(17)% with intensities of approximately 220/s and 11/s respectively. The main impurities at implantation were ^{17}C $\sim 0.5\%$ for the ^{19}N beam and ^{18}C $\sim 1.1\%$ the for ^{20}N beam. In addition, ^{16}C and ^{17}N beams were produced separately to calibrate the energy and efficiency of the neutron bar array. The purities of ^{16}C and ^{17}N were 99.7(1)% and 99.8(1)% respectively. The beams were transported to the decay monitoring system that consisted of an implantation detector, the neutron bar array and two HpGe detectors. The equipment has been used in similar measurements reported previously [18, 19].

TABLE I: Beam on and off time intervals.

Nuclide	Literature Half-life (s)	Beam on time (s)	Beam off time (s)
^{16}C	0.747(8)	1.5	3.0
^{17}N	4.173(4)	8.0	12.0
^{19}N	0.271(8)[a]	1.0	3.0
^{20}N	0.130(7)[a]	0.5/0.375[b]	0.8/0.375[b]

[a]Ref. [7]
[b]^{20}N beam was studied with two different settings

B. Implantation detector

The fragments of interest passed through a thin Kapton window, approximately 1 m of air, a 6 mm thick Al degrader, and a 300μm thick silicon surface barrier detector ($\triangle$E detector) before the ions were implanted in a thin plastic scintillator (implantation detector) placed at the center of the neutron bar array. The energy loss in the $\triangle$E detector combined with a time-of-flight measurement allowed on-line monitoring of the purities of the ^{19}N and ^{20}N beams. The start signal for all decay measurements was given by the implantation detector during the beam-off period. The second surface barrier detector (Veto detector) was placed after the implantation detector to monitor transmitted nuclei. The secondary beam was pulsed on for a fixed time period to collect nuclides in the implantation detector and the beta decay was monitored during the beam off time. The length of the time intervals, given in Table I, were based on the half-lives of the nuclides in each experiment.

C. Neutron bar array

The neutron bar array consisted of 16 plastic scintillator bars with a dimension of 157 cm $\times$ 7.6 cm $\times$ 2.54 cm. The detectors are arcs with a radius of 1 m to obtain an equal flight length for neutrons. The array was calibrated for time using an electronic time calibrator. The interaction flight path lengths for each bar were determined by the neutron time-of-flight measurements from ^{16}C and ^{17}N beta decays. These nuclei produce neutrons with well-known energies of 810, 1715 and 3290 keV from ^{16}C decay and 328, 1161 and 1721 keV from ^{17}N decay. The calibrated energy data from all bars were added in

order to produce the total neutron energy spectrum for each nuclide. The efficiency for the array was calibrated using peak areas from the total neutron energy spectra from ^{16}C and ^{17}N decays and known emission probabilities corresponding to each transition [18, 20]. Three additional efficiency data points were simulated using a Monte Carlo calculation with the detector geometry. The measured efficiencies were fitted as a function of energy. Fig. 1 shows the efficiency curve for the entire neutron array. The high energy part of the efficiency curve was obtained by extrapolating the linear region. The uncertainities of the efficiencies for energies higher than 1500 keV were about 3% and for energies less than 1500 keV, about 5%.

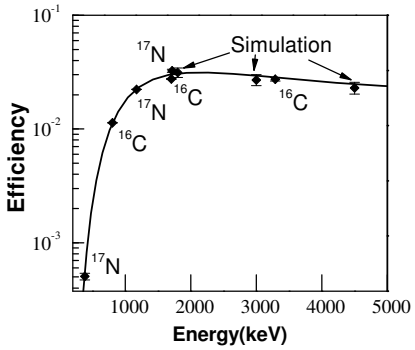

FIG. 1: The efficiency curve of the neutron array. The data points were obtained with ^{16}C and ^{17}N decay, and by simulation as indicated.

D. HpGe detectors

Two Hyperpure Germanium (HpGe) detectors with relative efficiencies of 120% and 80% were placed 12 cm and 10 cm from the implantation detector, respectively. Their readouts were triggered by the implantation detector. The 120% HpGe detector was set to observe gamma-rays within the window of 70-4000 keV. Gamma-rays with energies higher than 4000 keV were only detected using the 80% efficient HpGe detector. Off-line beta-gamma coincidence measurements using ^{60}Co, ^{134}Cs and ^{207}Bi sources with replacement of the implantation detector by a NaI(Tl) detector were performed to obtain the gamma-ray efficiency. In addition, well-know beta-gamma coincidences from the daughter decay of ^{19}N and ^{20}N and gamma-rays from ^{16}C and ^{17}N beta decays were used to augment the efficiency function. The efficiency value for the 197 keV gamma-ray from ^{19}O was excluded from the efficiency function due to the longer lifetime of this state compared to the master gate time width. Since the log(energy) verses log(efficiency) of the gamma-ray detectors was a straight line in the energy region of 600 keV to 3000 keV, it was extrapolated to higher energies. The low energy part of the efficiency function was obtained by scaling an efficiency function obtained in a previous off-line measurement to the 110 keV efficiency data point from the decay of ^{19}O. The uncertainties of efficiencies for energies higher than 500 keV were approximately 2% and for energies less than 500 keV were approximately 7%. Two HpGe detectors provided independent measurements of the gamma emission probabilities (except for 96 keV), which were averaged to produce final values.

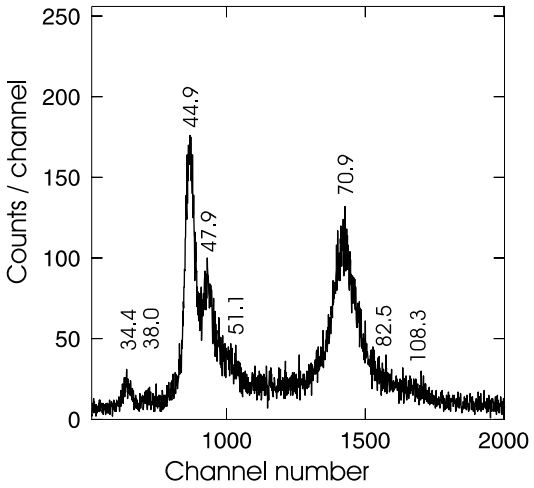

FIG. 2: Beta-delayed neutron time-of-flight spectrum of ^{19}N decay from one of the neutron bars. Time-of-flight corresponding to each peak is given in nanoseconds.

III. RESULTS AND DISCUSSION

The time-of-flight spectrum of beta-delayed neutrons from ^{19}N decay obtained from a single neutron bar is shown in Fig. 2 as an example of the raw data. The peak resulting from relativistic electrons that traveled from the implantation detector to the neutron bar provided a t=0 reference, not shown in the figure. The time measurements were calibrated using a TAC calibrator yielding a slope in the range of 0.035 to 0.038 ns/channel for all neutron detectors. The average flight lengths for neutrons from the implantation detector to the average interaction point in neutron bar were found to be in the range of 1.000 to 1.020 m for all neutron bars. The peak areas were obtained by fitting the neutron time-of-flight spectra with an asymmetric gaussian shape comprised of a gaussian function with an asymmetric parameter plus a polynomial background. The monotonic variation of the FWHM and the asymmetric parameter with time-of-flight were obtained from the ^{16}C and ^{17}N time-of-flight spectra.

A. Beta decay of ^{19}N

The total number of decay events for ^{19}N detected throughout the beam off period was extracted by fitting the decay curves. The ungated decay curve of ^{19}N was

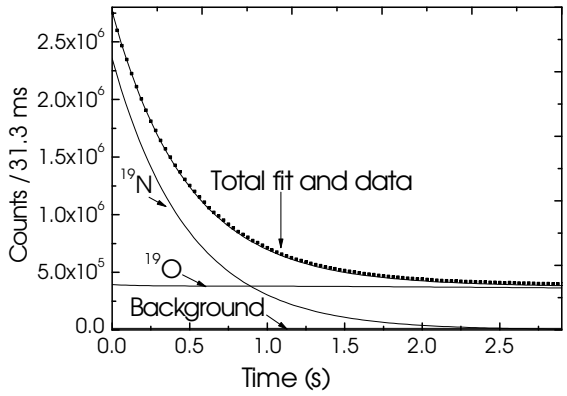

FIG. 3: The ungated beta decay curve of ^{19}N with the fitted function. The decay components of ^{19}N, ^{19}O and a constant background are labeled.

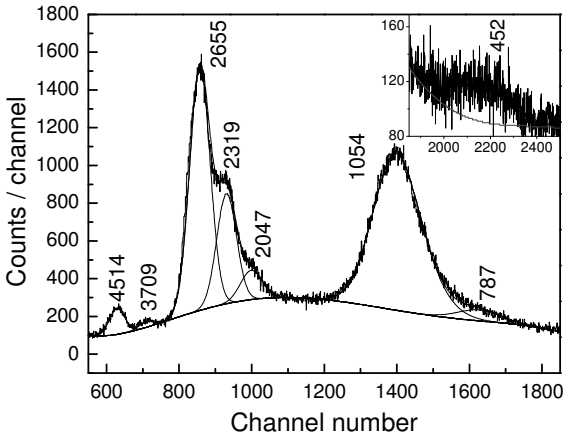

FIG. 4: Beta-neutron coincidence time-of-flight spectrum of ^{19}N. Peaks are labeled in keV. The low energy neutron peak is shown in the upper corner graph.

fitted, shown in Fig. 3, to a decay model derived from Bateman equations [21] for radioactive decay chain. This model includes the decay of ^{19}N, the growth and decay of ^{19}O during the beam off interval plus a constant background. The contribution from all growths and decays during the beam on period were taken into account to produce the decay during the beam off period. The fractions of nuclides that did not decay within a particular cycle were added to the next cycle. The constant background, which is small compared to the total decay, was defined by incorporating the half-life of the impurity ^{17}C and its implantation fraction. The half-life of ^{19}O beta decay ($T_{1/2}$ = 26.9 s) was fixed since it is known from previous work. Only the number of implanted nuclides, the half-life and the total neutron emission probability of ^{19}N beta decay were kept as variables throughout the fitting procedure, which define all decay components of the decay series. The total number of beta events was found

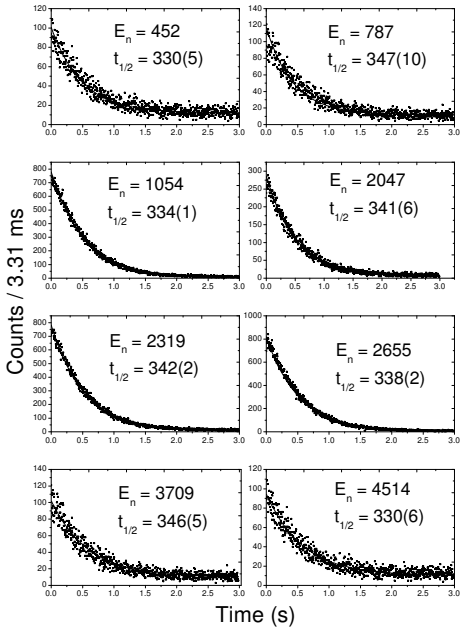

FIG. 5: Neutron gated decay curves of ^{19}N. All energies are given in keV.

to be $3.79(8) \times 10^7$ with a half-life of 338(5) ms, which is in agreement with the larger values from previous measurements [4, 6, 2], and a total emission probability of 39(8)% by fitting. The individual decay components derived from the fitted parameters are shown in Fig. 3. The beta-delayed neutron energy spectrum is shown in Fig. 4, where eight neutron groups at energies of 452(3), 787(3), 1054(4), 2047(10), 2319(11), 2655(13), 3709(21) and 4514(29) keV are labeled and are associated with ^{19}N decay. The spectrum was fitted with asymmetric gaussian functions with a third order polynomial for the background. The peak shapes were taken from the calibration including an asymmetric factor based on energy. An attempt was made to fit the spectrum without a peak at 787 keV. It was not possible to get a good fit under the constraints from the shape calibration. Decay curves were generated by placing a gate on each neutron peak to check the value of the gated half-life with the half-life of ^{19}N. Fig. 5 shows neutron gated decay curves fitted with a single decay component and a constant background. The gated half-lives from each peak are given in Table II and agree with the ungated half-life within error. The weighted average half-life derived from the neutron gated spectra was 336(2) ms. The neutron emission probability of each neutron group was calculated using the net peak area, neutron detection efficiency and the total number of observed decay events, and are presented in Table II with their uncertainties. The total neutron emission probability was found to be 41.8(9)% by adding all neutron branch probabilities. This is in agreement, within the large errors, with previous values measured by Reeder and Mueller. The assignment of beta-delayed neutron transitions will be addressed below.

Fig. 6 shows the gamma-ray spectrum measured in co-

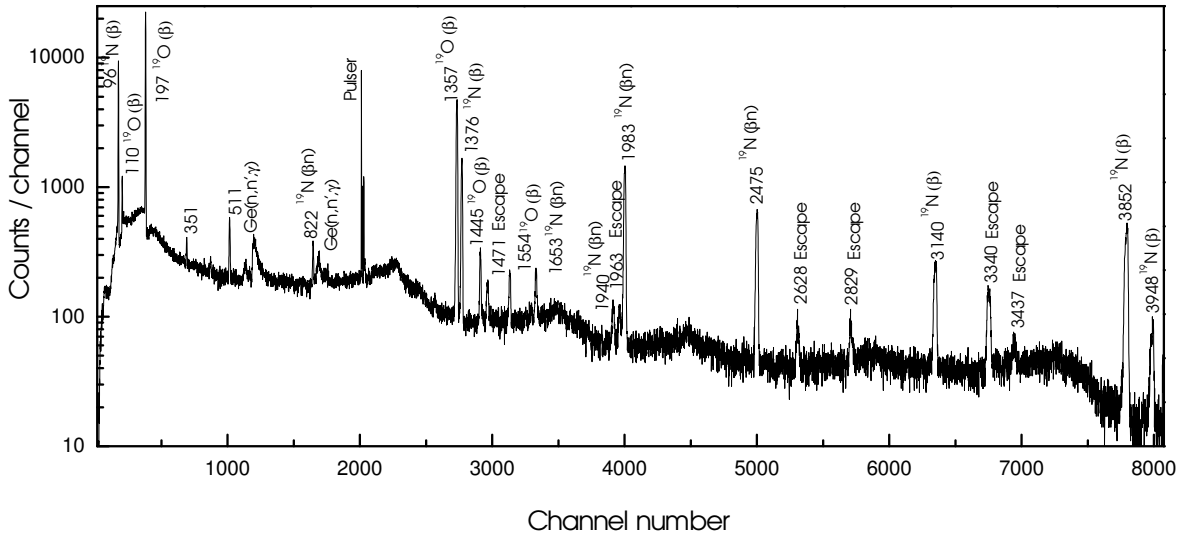

FIG. 6: The beta-gamma coincidence spectrum from ^{19}N beta decay. Energies are given in keV and peaks are labeled with the parent nuclide and the decay mode. The gamma peaks due to the neutron reactions in Ge are shown. The escape peaks are labeled separately.

TABLE II: Neutron emission probabilities of ^{19}N beta decay.

Energy (keV)	Gated half-life(ms)	Neutron emission probability(%)
452(3)	330(5)	10.4(8)
787(3)	347(7)	0.9(1)
1054(4)	334(1)	17.3(4)
2047(10)	341(6)	1.2(1)
2319(11)	342(2)	4.1(1)
2655(13)	338(2)	6.7(2)
3709(21)	346(5)	0.3(1)
4514(29)	330(6)	0.9(1)
Total emission probability		41.8(9)%
Reference	Predicted half-life	Predicted Neutron emission probability(%)
Warburton	0.54(s)	87%
Brown	289(ms)	85.6%

incidence with the beta decay of ^{19}N during the beam-off intervals. The gamma transition energies at 110.5(3), 1357.2(5), 1444.6(5) and 1554.4(5) keV from ^{19}O beta decay, the daughter of ^{19}N, were observed with gamma emission probabilities of 2.7(1), 50.1(14), 2.6(1) and 1.7(1)% respectively. These values are in agreement with literature values [12,22] and are labeled as ^{19}O(β) in Fig. 6. The gamma-ray at 197.8(3) keV was also detected from the same decay and the emission probability disagrees with literature value. The reason for the disagreement is the short coincidence time of the master gate in this work compared to the mean lifetime (197 ms) of the 197.8 keV state. The gamma-ray energies of 96.4 and 3139 keV from ^{19}N beta decay reported by Dufour et al. [2] were observed and agreed within errors. The gamma-ray at 709.2 keV measured by the same group was not observed in our experiment with a detection limit of 0.05(8)% for gamma emission at this energy. This nonobservation supports the argument made by Hubert et al. [8] and Weissman et al. [9] that the 709.2 keV gamma-ray energy is not produced by ^{19}N beta decay based on their gated half-life measurement and should be assigned to contaminant ^{22}O beta decay in the previous measurement. There are four broad peaks at energies of 569, 583, 843 and 869 keV observed due to the neutron interactions with the Ge detector. Three gamma-ray energy lines at 351, 665 and 740 keV are observed from the neutron reactions with surrounding metals. The remaining gamma-ray energies were assigned on the basis of the gamma gated half-lives, the compatibility of energy differences between experimentally known energy levels of daughters, intensity match through the decay flow, and observation of peaks in the beta-gamma-neutron coincidence spectra. The half-lives obtained from the gamma gated decay curves, shown in Fig 7, for gamma rays associated with ^{19}N decay are given in Table III. The weighted average half-life from all of the gamma gated decay curves is 329(6) ms. The consistency of half-lives with the ungated half-life confirms that the above gamma-ray energies can be attributed to the beta decay of ^{19}N decay. The analysis of triple coincidence spectra showed that the 1983 keV transition follows the beta-delayed neutron decay. In addition, the gammas at 821.6, 1652.4 and 1939.7 keV can be assigned to transitions between ^{18}O levels based on their consistency with energy differences between experimentally known levels. The gamma-ray energy of 1982.9

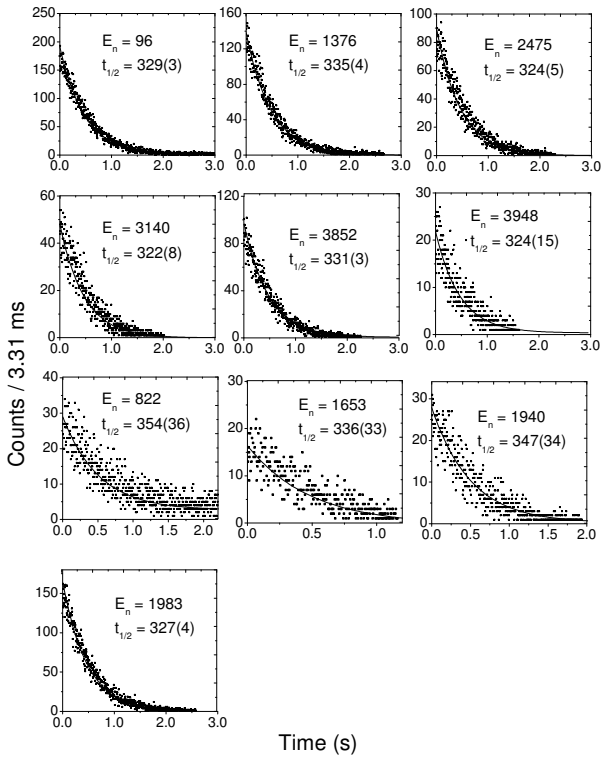

FIG. 7: Gamma gated decay curves of ^{19}N. All energies are given in keV. The half-lives obtained by fitting are given in milliseconds.

keV is placed at the known energy level at 1983.0 keV (J^π=2^+) in ^{18}O. This level is fed by gamma transitions with 1652.4 and 1939.7 keV from the 3634 (J^π=0^+) and 3920 keV (J^π=2^+) levels, respectively. The transition at 821.6 keV was assigned to the decay of the level at 4458 keV (J^π=1^-) in ^{18}O. The transition at 2475.2 keV could have two sources; this energy is consistent with the $1^-\rightarrow 2^+$ transition in ^{18}O and also with the $3/2^-\rightarrow 1/2^+$ transition in ^{19}O. The 821.6 and 2474.2 keV gamma transitions from the 4458 keV level in ^{18}O should have an absolute intensity ratio of approximately 13:5 and the observed intensity ratio was 1:13. Therefore, the strong 2474 keV gamma transition was assigned to ^{19}O. The remaining gamma energies in the spectrum were assigned to transitions in ^{19}O based on previous knowledge of the level scheme [12].

The excited states of ^{19}O have been studied using ^{13}C(^{7}Li,p)^{19}O, ^{17}O(t,p)^{19}O, ^{18}O(n,γ)^{19}O and ^{18}O(d,p)^{19}O reactions [12,23,24]. Most of the states with energies lower than 6000 keV are known with an uncertainty of 0.5% from the above studies. The knowledge of these energy levels was used to assign the observed gamma-ray energies of 1375.7, 2475.2, 3851 and 3947 keV to transitions among the ^{19}O energy levels. They are labeled as ^{19}N(β) in Fig. 6 and Table III. Although the gamma transition of 1471.3(5) keV could be assigned to the state at 1472 (J^π=$1/2^+$) based on energy, it is the escape peak of the gamma-ray at 1982.9 keV. A transition with this energy was not assigned to the beta decay of ^{19}N. In addition, the agreement between the gamma gated half-lives (Table III) with the half-life obtained from the ungated decay curve confirms the above decay assignments. The gamma emission probabilities, given in Table III, were calculated using peak areas, the gamma detection efficiency and the total number of ^{19}N decay events observed.

TABLE III: Gamma emission probabilities of ^{19}N beta decay.

Energy (keV)	Nuclide	Gated half-life(ms)	Decay assignment	Emission probability%
96.4(3)	^{19}O	329(3)	^{19}N(β)	47.4(13)
1375.7(5)	^{19}O	335(4)	^{19}N(β)	17.2(5)
2475.2(7)	^{19}O	324(5)	^{19}N(β)	15.6(5)
3139(1)	^{19}O	322(8)	^{19}N(β)	8.1(3)
3851(1)	^{19}O	331(3)	^{19}N(β)	22.0(8)
3947(1)	^{19}O	324(15)	^{19}N(β)	3.4(2)
821.6(3)	^{18}O	354(36)	^{19}N(βn)	1.2(1)
1652.4(5)	^{18}O	336(32)	^{19}N(βn)	1.9(1)
1939.7(6)	^{18}O	347(34)	^{19}N(βn)	1.1(1)
1982.9(6)	^{18}O	327(4)	^{19}N(βn)	27.1(8)

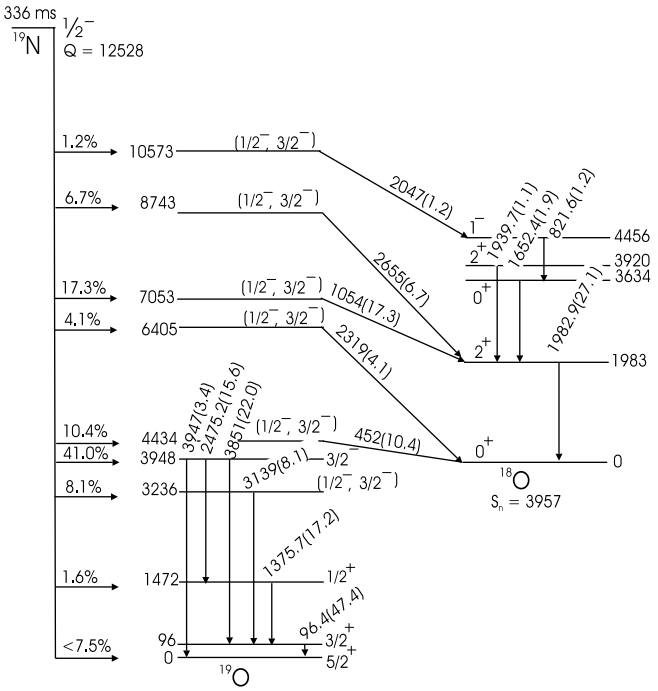

FIG. 8: The decay scheme of ^{19}N beta decay. All energies are given in keV. The beta decay branches are given as percentages. The neutron transition energies are shown on the transition line with their emission probabilities in parenthesis. The weighted average half-life derived from all gated half-life measurements are shown

The beta-delayed neutron transitions deduced in this work are shown with the gamma ray transitions in Fig. 8. The neutron energies and their probabilities had to match with known states in the daughter combined

TABLE IV: The comparison of experimental and shell model calculations for ^{19}N beta decay.

Experiment					Shell model calculation									
					WBP[a]					MKIII[b]				
Energy (keV)	Spin Parity	Branch (%)	Log(ft)	B(GT) ×1000	Energy[a] (keV)	Spin Parity	Branch (%)	Log(ft)	B(GT) ×1000	Energy[b] (keV)	Spin Parity	Branch (%)	Log(ft)	B(GT) ×1000
0	$5/2^+$	<7.5	>6.20	<3.9						0	$5/2^+$	1.02	7.0	0.6
96	$3/2^+$	0								96[c]	$3/2^+$	0.49	7.30	0.3
1472	$1/2^+$	1.6	6.71	1.2						1472[c]	$1/2^+$	4.88	6.06	5.4
3236	$1/2^-$,$3/2^-$	8.1	5.62	14.8	2247	$1/2^-$	6.5	5.9	5.2	3232[c]	$1/2^-$,$3/2^-$	1.1	6.77	1.0
					4048	$1/2^-$	7.9	5.4	15.9					
					4678	$1/2^-$	17.2	4.9	49.7					
3948	$3/2^-$	41.4	4.75	109.8	4801	$3/2^-$	3.4	5.6	10.6	3945[c]	$3/2^-$	6.2	5.86	8.5
4434	$1/2^-$,$3/2^-$	10.4	5.22	37.2	5719	$3/2^-$	0.9	5.8	5.1	4582	$1/2^-$	3.4	5.97	6.6
										5082	$1/2^-$	39.2	4.77	104.9
6405	$1/2^-$,$3/2^-$	4.1	5.05	55.1	6255	$1/2^-$	1.8	5.4	14.4	6755	$3/2^-$	12.7	4.75	109.8
					6326	$3/2^-$	25.3	4.2	22.0					
					6437	$3/2^-$	6.3	4.8	59.6					
7053	$1/2^-$,$3/2^-$	17.3	4.19	398.8	7190	$3/2^-$	4.2	4.7	73.3	7119	$3/2^-$	4.3	5.08	51.4
					7377	$3/2^-$	0.8	5.4	16.6	7509	$3/2^-$	12.2	4.49	199.9
					7774	$1/2^-$	0.5	5.4	15.5	7622	$1/2^-$	1.3	5.42	23.5
					7784	$3/2^-$	4.5	4.5	13.4	7843	$3/2^-$	3.7	4.87	83.3
8743	$1/2^-$,$3/2^-$	0.9	4.71	120.4	8155	$3/2^-$	7.1	4.1	30.7	8196	$3/2^-$	5.4	4.55	172.6
					8289	$1/2^-$	7.3	4.0	36.4	8505	$1/2^-$	3.6	4.57	166.9
					8656	$3/2^-$	2.0	4.4	15.0	8506	$3/2^-$	2.5	4.74	111.2
10573	$1/2^-$,$3/2^-$	1.2	3.37	2635	9638	$3/2^-$	0.7	4.3	20.2					

[a]Calculated by Brown for negative parity states
[b]Calculated by Warburton using MKIII interaction
[c]Experimental energies were used in Ref.[15]

with the observed gamma-ray transitions and their probabilities. The neutron energies of 1054 and 2655 keV have been assigned to feed the 1983 keV energy level in ^{18}O due to the high feeding required by 1983 keV gamma transition. Two neutron transitions of 452 and 2319 keV go to the ground state of ^{18}O without emitting any subsequent gamma-rays. The neutron energy of 2047 keV was assigned to feed the gamma transition from the 4456 keV in the ^{18}O. The neutron energies with the emission probabilities less than 1.0% were not assigned to energy levels in ^{19}O due to the fact that these neutrons can be placed in several ways and still match the gamma transitions among ^{18}O levels. The overall decay scheme of ^{19}N beta decay, shown in Fig.8, combines the neutron and gamma emission probabilities, and their decay assignments. The emission probabilities are given in parenthesis following the transition energy. The gamma emission probabilities following beta-delayed neutron decay are consistent within errors with the neutron emission probabilities measured independently by the neutron array. The branching percentages to energy levels in ^{19}O shown at the left of Fig. 8 were calculated by combining gamma and neutron decay information. The upper limit of beta decay branch feeding the ground state of ^{19}O is estimated from branches feeding excited states, which are observed through gamma and neutron emission, and emission probabilities from the unassigned neutron groups. The beta decay half-life for ^{19}N derived from all gated half-life measurements is given at the top of Fig. 8.

The log(ft) values and Gammow-Teller transition strengths (B(GT)) were calculated for all beta decay branches using methods described in Ref.[25,26], respectively. The values are given in Table IV with the corresponding values from shell model calculations. The experimental log(ft) values are based on observed neutron and gamma transitions, and thus should be considered provisional due to the possibility of unobserved transitions. The spins and parities for experimental levels were deduced based on log(ft) values and beta decay selection rules with consideration of beta decay systematics in this region. The spins and parities for the energy levels of 0, 96 and 1472 keV were previously found to be $5/2^+$, $3/2^+$ and $1/2^+$ respectively [12,23,24]. The observed log(ft) values indicate that beta decay to these levels can be categorized as first forbidden decay confirming the assignments. But the small log(ft) value for the 3236 keV level indicates that it could be an allowed decay to a negative parity state. The beta decay rules limit the spin and parity to $1/2^-$ and $3/2^-$ for this level, considering the ground state of ^{19}N has a spin and parity of $1/2^-$. This assignment supports a similar argument made by Warburton [15] but disagrees with measurements using the ^{13}C(^{7}Li,p)^{19}O, ^{17}O(t,p)^{19}O and ^{18}O(d,p)^{19}O reactions. The experimentally known $J^\pi=3/2^-$ state at 3948 keV has the highest branch with a log(ft) value of 4.75,

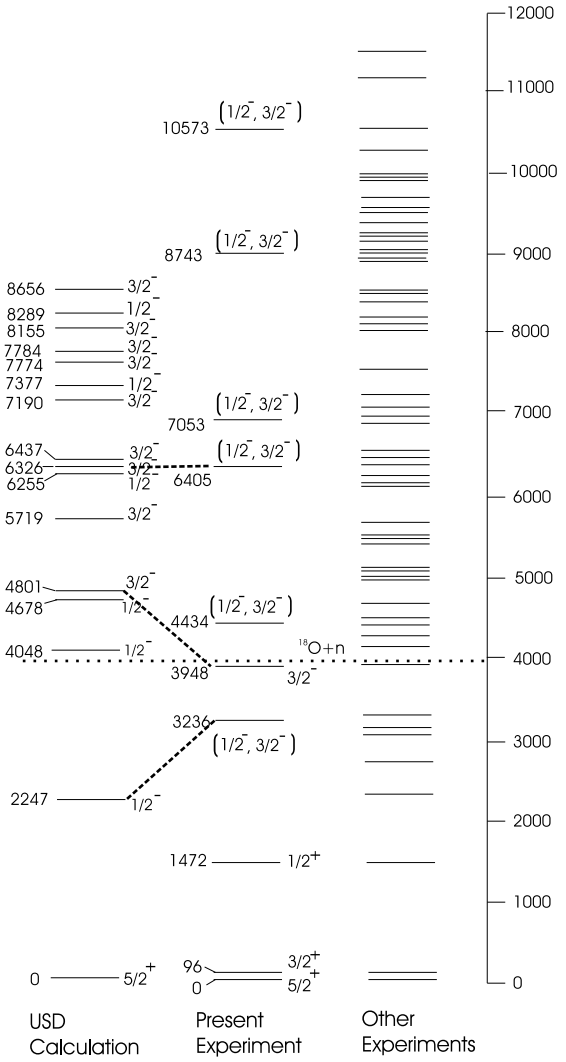

FIG. 9: Comparison of experimental and calculated excited states of ^{19}O. All energies are given in keV. The allowed negative parity energy states calculated using the WBP interaction in a *sp-sd* model space are given in the first column. The energy levels extracted from this experiment are given in the second column. The last column shows the energy levels obtained from other experiments using direct reactions. The dotted line shows the single neutron separation energy of ^{19}O.

which also indicates allowed beta decay. The energy levels higher than 7000 keV are experimentally unknown and have log(ft) values in the range of 2.82 - 4.75 from this experiment. They should be allowed decay based on their log(ft) values and systematics of ^{17}N decay.

The proposed spins and parities for observed energy levels above the neutron separation energy are $J^\pi=1/2^-$ or $3/2^-$. The comparison between experimental values and theoretical calculations for beta decay shows large differences in the major beta branches. Our measurements indicate that four neutron bound states and five neutron unbound states are fed by ^{19}N beta decay. The comparison between the deduced levels from this experiment and shell model predictions for allowed beta decay by Brown [16] are given in Fig. 9. The energies having branching ratios greater than 1% from the theoretical calculations are shown along with the levels measured from previous experiments for comparison purposes. The likely candidates for the lowest experimental energy levels and shell model predictions with $J^\pi=1/2^-$ and $3/2^-$ assignments are connected by dashed lines.

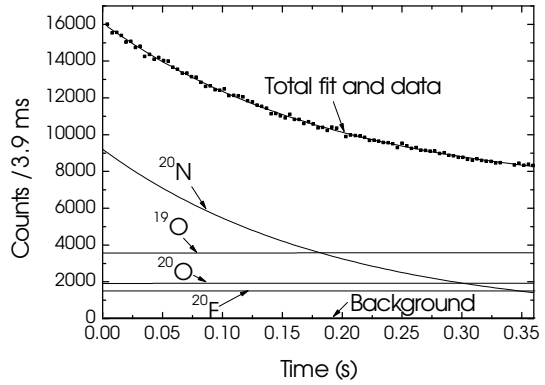

FIG. 10: The ungated beta decay curve of ^{20}N with the fitted function. The decay components of ^{20}N, ^{20}O, ^{20}F, ^{19}O and a constant background are labeled.

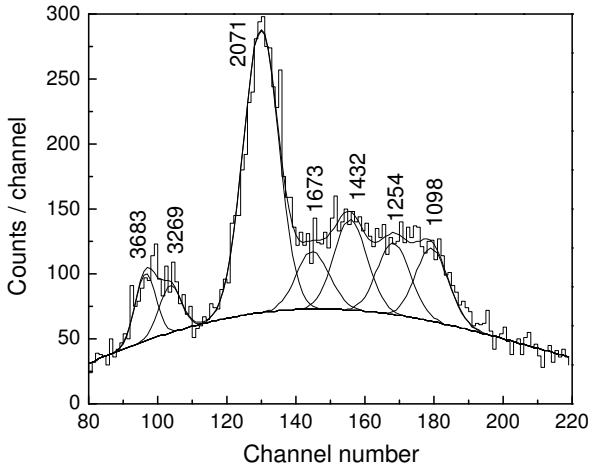

FIG. 11: Beta-neutron coincident time-of-flight spectrum of ^{20}N. All energies are given in keV. The fitted asymmetric gaussian peaks are shown with a smooth polynomial background.

B. Beta decay of ^{20}N

The total number of ^{20}N decay events was determined by fitting the ungated decay curve, shown in Fig. 10, with a model that included the beta decay of ^{20}N, the growth and decay of ^{20}O, ^{20}F and ^{19}O and a constant

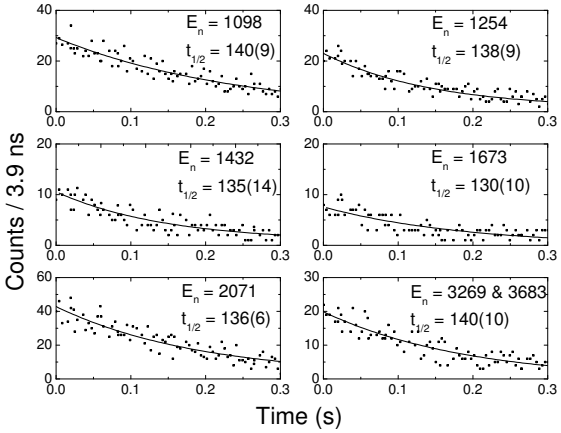

FIG. 12: The neutron gated decay curves of ^{20}N. The energies and half-lives are given in keV and milliseconds.

TABLE V: Neutron emission probabilities of ^{20}N beta decay.

Energy (keV)	Gated half-life (ms)	Neutron emission probability(%)
1098(1)	140(9)	7.6(7)
1254(2)	138(9)	5.2(5)
1432(2)	135(14)	4.4(5)
1673(4)	130(10)	4.3(6)
2071(2)	136(6)	14.9(6)
3269(7)	140(10)	2.5(7)
3683(5)	140(10)	4.5(5)
Total emission probability		42.9(14)%
Reference	Predicted half-life	Predicted neutron emission probability(%)
Brown	118(ms)	71.1

TABLE VI: Gamma emission probabilities of ^{20}N beta decay.

Energy (keV)	Nuclide	Decay Assigment	Emission probability
1674.4(5)	^{20}O	^{20}N(β)	51.6(11)
1812.1(6)	^{20}O	^{20}N(β)	2.9(7)
1898.2(6)	^{20}O	^{20}N(β)	6.5(7)
2397.0(7)	^{20}O	^{20}N(β)	7.1(8)
2779.5(9)	^{20}O	^{20}N(β)	1.4(6)
2982(1)	^{20}O	^{20}N(β)	2.1(5)
3497(1)	^{20}O	^{20}N(β)	3.4(8)
4072(2)	^{20}O	^{20}N(β)	2.2(7)
4882(3)	^{20}O	^{20}N(β)	2.2(7)
5896(4)	^{20}O	^{20}N(β)	4.3(10)
96.4(3)	^{19}O	^{20}N(βn)	43.9(19)
1375.5(5)	^{19}O	^{20}N(βn)	15.6(7)

background. The model was derived using Bateman eqations with three variables that are the number of implanted nuclides, the half-life and the total neutron emission probability of ^{20}N. The fitted function used fixed beta decay half-lives for the two daughters and granddaughter ($T_{1/2}$ =13.5 s for ^{20}O, $T_{1/2}$ = 11.1 s for ^{20}F, $T_{1/2}$ = 26.9 s for ^{19}O) with a constant background defined by the beta decay of ^{18}C and its implantation fraction. The number of beta events observed was found to be $7.42(2) \times 10^5$ with a half-life of 133(5) ms, which is consistent with all except the earliest previous results [4 - 7].The total neutron emission probability was found to be 46(11)%. The individual decay contributions from the daughters and the granddaughter are shown in Fig. 10. The beta-delayed neutron time-of-flight spectrum is shown in Fig. 11, where the neutron peak energies are labeled in keV. Seven neutron peaks at 1098(1), 1254(2), 1432(2), 1673(4), 2071(2), 3269(6) and 3683(5) keV are needed to fit the observed data based on the predetermined peak shapes. The flat region of the time-of-flight spectrum near channel 160 was fitted with only three peaks as a test. The peaks had larger FWHM values, inconsistent with the peak shape calibration and were rejected. The neutron gated half-lives were used to confirm the assignment of the beta-delayed neutrons. The neutron gated decay curves are given in Fig. 12, which were fitted with an exponential component and a constant background. The half-lives extracted from the gated decay curves are given in Table V and the weighted average of the half-lives is 137(3) ms. The observed neutron emission probabilities with their uncertainties are given in Table V. The total neutron emission probability was found to be 42.9(14)%.

The beta-gamma coincidence spectrum is given in Fig. 13, which was obtained using the 120% HpGe detector during the beam-off time intervals. The beta-gamma coincidence spectrum from the 80% HpGe detector for the higher energy range (4000-6000 keV) is shown in Fig. 14. The gamma-rays from the daughter decay of ^{20}O and granddaughter decay of ^{20}F were observed at 1059 and 1634 keV, respectively in agreement with literature values [27]. Four gamma-ray energies of 110.5, 197.8, 1357.2 and 1444.6 keV were observed from beta decay of ^{19}O and they are also in agreement with literature values [22]. As in the ^{19}N gamma spectrum, the gamma-rays due to neutron interactions with the Ge crystal and surrounding metals were observed and they are labeled in the spectrum. The assignments for all above gamma-ray energy lines were confirmed by their gamma gated half-lives. Gamma-gated decay curves were obtained for the 1674.2(5) and 96.3(3) keV lines with sufficient statistics to identify the decay. They were fitted with single exponential decay and a constant background. The gated half-lives obtained as 135(5) and 138(9) respectively and the weighted average of gamma gated half-life was 136(5) ms. The counting statistics for gamma energies of 1375.5(5), 1812.1(6), 1898.2(6), 2397.0(7), 2779.5(9), 2982(1), 3497(1), 4072(2), 4882(3) and 5896(4) keV were too low to allow determination of the gated half-lives. They were assigned to the decay of ^{20}N based on the energy differences of known energy levels of ^{20}O

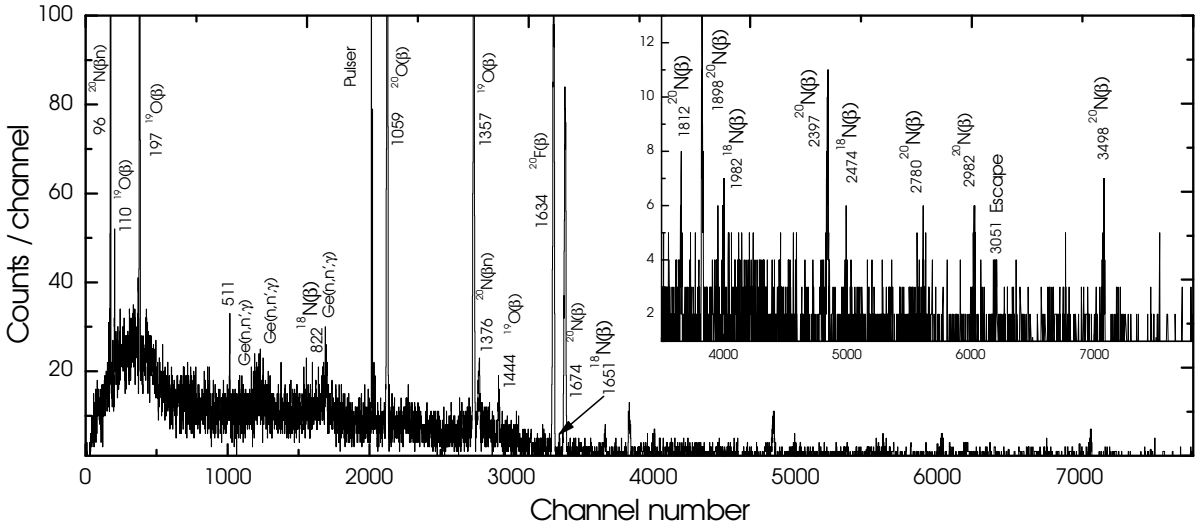

FIG. 13: The beta-gamma coincidence spectrum of ^{20}N beta decay. The energy is given in keV with the parent nuclide with decay mode. The gamma peaks due to neutron reaction with Ge crystal are shown, similar to Fig. 6.

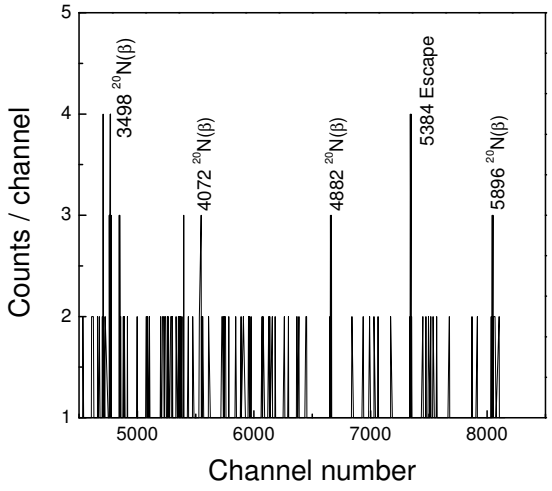

FIG. 14: The high energy beta-gamma coincidence spectrum of ^{20}N beta decay from 80% HpGe detector. The energies are given in keV. The peaks are labeled with the parent nuclide and decay mode.

and considering the branching ratios. Two transitions at 96.3(2) and 1375.5(3) keV were identified as gamma transitions in ^{19}O levels following beta-delayed neutron emission. The gamma peaks at 822.1, 1651.3, 1982.4 and 2474.1 keV were attributed to ^{18}N beta decay, which is produced from the beta decay of the impurity ^{18}C, based on intensity ratios of the peaks [12]. Other features that are not labeled in Fig. 14 are not considered peaks, as they have unreasonably small FWHM's. The remaining gamma energies were assigned to ^{20}O levels on the basis of their energies. The emission probabilities produced by averaging the two independent measurements from the HpGe detectors, are given in Table VI with their assignments.

The energy levels in ^{20}O were determined by LaFrance et al.[10] using the ^{18}O(t,p)^{20}O reaction, by Stanoiu et al.[13] using single step fragmentation process, by Tryggestad et al.[28] using coulomb excitation and recently by Wiedeking et al.[14] using ^{10}Be(^{14}C,α)^{20}O reaction. The energy levels below 8000 keV are relatively well-known and they were used as a basis for gamma-ray placement among the ^{20}O energy levels. The gamma-ray energy of 1674.2 keV is assigned to the transition between the known energy level at 1674.2 (J^π=2^+) keV and the ground state. Five gamma transitions with energies of 1898.2, 2397.0, 2779.5, 4882 and 5896 keV cascade to the first J^π=2^+ state from energy levels at 3573 (J^π=4^+), 4072 (J^π=2^+), 4455 (J^π=0^+), 6556 (J^π=2) and 7570 keV, respectively. The energy level at 3573 keV is fed by gamma transitions of 1812.1 and 2982 keV from the energy levels at 5384 (J^π=0^+) and 6556 (J^π=2) keV, respectively. The gamma-ray energies of 4072 and 5896 keV were taken to originate from the 4072 (J^π=2^+) and 7570 keV energy levels, respectively. The gamma-ray energy of 3497 keV is assigned to the feeding from the 7570 keV level. The gamma-ray of 5384 keV is identified as an escape peak, which is not assigned to the energy level at 5384 (J^π=0^+).

The beta-delayed neutron transitions were placed on the basis that the observed gamma transitions in ^{19}O need to be fed by neutron transitions. First, the observed gamma energies of 96.4 and 1375.5 keV were assigned to the 96 (J^π=$3/2^+$) and 1472 (J^π=$1/2^+$) keV levels in ^{19}O, respectively, based on the knowledge from our measurements of the beta decay of ^{19}N. The neutron transitions were placed in order to fulfill the feeding requirements of these energy levels. Three neutron transitions of 1098, 1254 and 2071 keV fed into the 96

TABLE VII: The comparison of experimental and shell model calculation for ^{20}N beta decay.

Experiment					Shell model calculation				
Energy (keV)	Spin Parity	Branch (%)	Log(ft)	B(GT) ×1000	Energy (keV)	Spin Parity	Branch (%)	Log(ft)	B(GT) ×1000
0	[a] 0^+	<3.3	>7.09	<0.5					
1674	[a] 2^+	30.1	5.90	7.8					
3573	[a] 4^+	1.5	6.92	0.7					
4072.0	[a] 2^+	5.9	6.25	3.5					
4455.5	[a] 0^+	1.4	6.81	1.0					
5383.9	[a] 0^+	2.9	6.34	2.8	5051	1^-	4.7	6.1	3.1
6556.7	[b] 2^+	4.3	5.95	6.9	5325	2^-	1.1	6.7	0.8
					6131	2^-	15.2	5.4	15.1
					6152	1^-	3.6	6.0	3.6
					6920	2^-	1.2	6.4	1.7
7570	1^-,2^-,3^-	7.7	5.49	20.0	7232	1^-	1.6	6.2	2.5
					7736	1^-	2.8	5.8	5.6
8860	1^-,2^-,3^-	7.6	5.19	39.9	8157	3^-	1.3	6.1	3.3
					8400	3^-	9.2	5.2	25.4
					8437	2^-	2.7	5.7	7.6
					8548	2^-	3.5	5.6	10.3
					8791	3^-	2.4	5.7	7.9
					8873	2^-	1.4	5.9	4.7
9024	1^-,2^-,3^-	5.2	5.31	30.3	9463	2^-	1.2	5.8	5.8
9884	1^-,2^-,3^-	14.9	4.64	141.5	9586	3^-	1.1	5.8	5.8
					9728	2^-	1.9	5.6	10.7
10587	1^-,2^-,3^-	4.4	4.97	66.2	10006	2^-	1.3	5.7	8.4
10841	1^-,2^-,3^-	4.3	4.91	76.0	10219	1^-	2.0	5.4	14.6
					10622	3^-	2.2	5.3	21.0
					10664	2^-	4.4	5.0	43.5
					10884	2^-	2.9	5.1	33.4
					11188	2^-	2.8	5.0	38.6
					11834	3^-	2.3	4.9	50.9
					11886	1^-	1.6	5.0	36.6
12521	1^-,2^-,3^-	2.5	4.46	384.2	12367	2^-	1.7	4.8	58.3
12957	1^-,2^-,3^-	4.0	4.18	452.7	12367				

[a]Experimentally known spin and parity
[b]Parity was determined in present work

($J^\pi=3/2^+$) keV level in ^{19}O while the rest of the neutrons feed the 1472 ($J^\pi=1/2^+$) keV level. The average gamma emission probabilities measured by two HpGe detectors are 43.9(19) and 15.6(7)% for 96 and 1375 keV gamma transitions, respectively, are in good agreement within the uncertainties with neutron emission probabilities independently measured by the neutron array.

Fig. 15 shows the suggested decay scheme for the beta decay of ^{20}N. The beta branching percentages to energy levels in ^{20}O are calculated by considering the observed neutron and gamma emission probabilities, and their assignments. The upper limit of beta decay to the ground state of ^{20}O is estimated based on beta decay branches feeding to the observed energy levels. The energy level at 1674 keV has the highest beta decay branch of 30.1% and the neutron unbound energy level at 9884 keV has the second highest beta decay branch of 14.9%. The log(ft) values and Gammow Teller strengths were calculated for each beta branch based on the observed neutron and gamma transitions in order to assign spins and parities. The log(ft) values should be considered provisional due to the posibility that some transitions were not observed. Table VII gives the experimental values and a comparison to shell model calculations [16] for branching ratios, log(ft) and B(GT) values. The beta decay to the energy levels higher than 7500 keV are considered to be allowed decay based on their log(ft) values and according to the systematic behavior of the log(ft) values in this region. The log(ft) values for these transitions are in the range of 4.18 - 5.49 and the spins and parities are suggested as $J^\pi=1^-$, 2^-, 3^- based on the beta decay rules assuming that the ground state of ^{20}N has a spin and parity of 2^-. The log(ft) values corresponding to the observed energy levels lower than 7500 keV are in the range of 5.90 - 7.10 and indicate that the beta decays are first forbidden. The spins and parities for these levels are experimentally known [10,13,14] except for the parity of the 6556 keV level and they are in agreement with our assignments. The parity for the 6556 keV level is assigned as positive considering the first forbid-

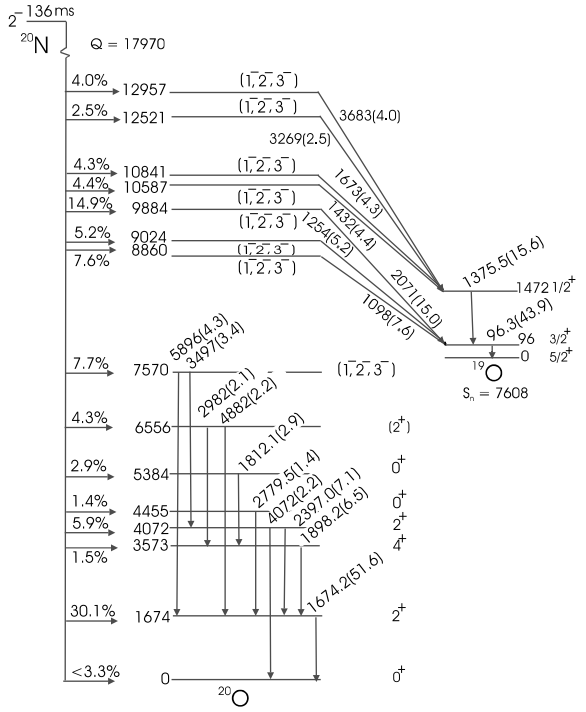

FIG. 15: The beta decay scheme of ^{20}N. Transition energies and their emission probabilities in parentheses are given. Beta branching ratios are shown in the left as horizontal arrows with percentages. All energies are given in keV. The weighted average half-life derived from all gated half-lives are shown.

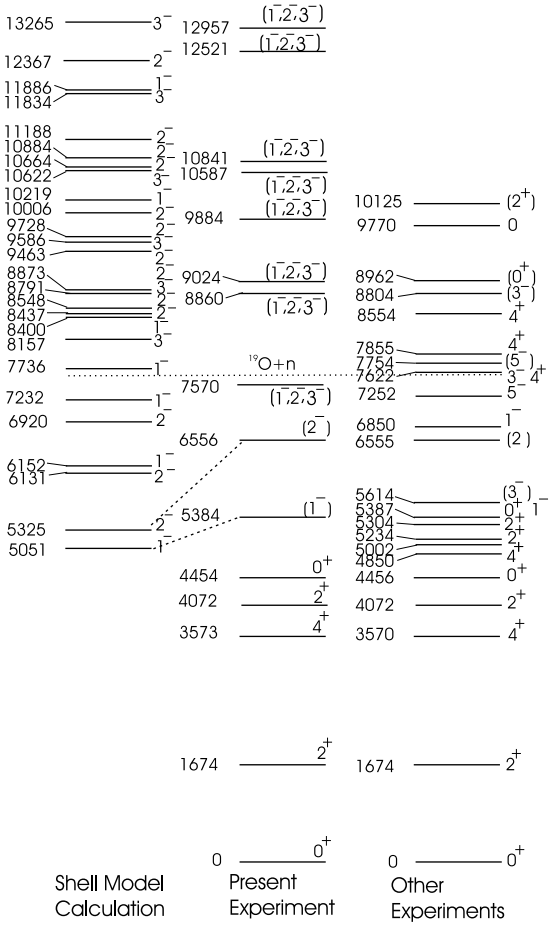

FIG. 16: The energy level scheme of ^{20}O. The ^{20}O level scheme obtained from the shell model calculations for negative parties (left column), the present work (middle column) and from literature (right column) are shown with their parities. All energies are given in keV.

den beta decay selection rules. The energy levels deduced from our measurements are compared with negative parity states from the shell model calculations, shown in Fig. 16. In addition, the adopted energies from other experiments are shown for comparison. The positive parity states below 7000 keV are in good agreement within errors with the adopted energies. Four new energy levels at 10587, 10841, 12521 and 12957 keV are observed, which are higher than the highest energy level determined by previous experiments. The energy difference between the first negative parity state predicted by shell model calculations and the present experiment is 333 keV. Fig. 16 shows the energy levels corresponding to allowed beta decay predicted by the shell model have a poor agreement with the experimental values.

IV. CONCLUSION

The present work reports the first beta delayed neutron spectroscopic study of ^{19}N and ^{20}N. Eight neutron energies with ten gamma transitions were observed for ^{19}N beta decay. The weighted average half-life from all gated half-life measurements was 336(3) ms and the total neutron emission probability was 41.8(9)% for the ^{19}N beta decay. Seven energy states in ^{19}O, with allowed beta decay feeding were observed from the ^{19}N beta decay. These states are fed 90.9% of the total decay and in which 46.0% feed neutron unbound states. The first forbidden decays to two energy levels were observed with an upper limit of 9.1% of the total decay. Seven neutron energies and twelve gamma transitions were observed from the ^{20}N beta decay. The total neutron emission probability and the weighted average half-life obtained from all gated half-life measurements were 42.9(14)% and 136(3) ms for ^{20}N beta decay, respectively. The allowed beta transitions, which are 50.6% of the total decay, feed eight energy levels in ^{20}O and 84.8% of these decays feed neutron unbound states. The first forbidden transitions feed seven positive parity states.

Acknowledgments

We would like to thank Dr. B. A. Brown for providing the shell-model calculations and the staff of the NSCL for their assistance during experiments. This work was sup-

ported by the National Science Foundation under grants PHY-94-03666 and PHY-01-10253.

[1] D. W. Anthony *et al.*, Origin of Elements in the Solar System: Implications of Post-1957 Observations, Proc. Int. Sym.; Kluwer Aca/Plenum Publishers, p.51 (2000).
[2] J. P. Dufour *et al.*, Z. Phys. **A324**, 487 (1986).
[3] J. P. Dufour *et al.*, Proc. 5^{th} Int. Conf. Nuclei Far from Stability, Canada, Ed. I. S. Towner p. 344 (1988).
[4] A. C. Mueller and P. L. Reeder, Z. Phys. A -Atomic Nuclei **A330**, 63 (1988).
[5] M. Samuel *et al.*, Phys. Rev. C **37**, 1314 (1988).
[6] P. L.Reeder *et al.*, Phys. Rev. C **44**, 1435 (1991).
[7] P. L. Reeder *et al.*, Proc. Int. Conf. on Exotic Nuclei and Atomic Masses, France, p. 587 (1995).
[8] F. Hubert *et al.*, Z. Phys. A -Atomic Nuclei **333**, 237 (1989).
[9] L. Weissman *et al.*, J. Phys. G: Nucl. Part. Phys. **31**, 553 (2005).
[10] S. LaFrance, H. T. Fortunee, S. Mordechai, M. E. Cobern, G. E. Moore, R. Middleton, W. Chung, and B. H. Wildenthal, Phys. Rev. C **20**, 1673 (1979).
[11] K. C. Young Jr. *et al.*, Phys. Rev. C **23**, 980 (1981).
[12] R. B. Firestone (2002), John Wiley and Sons, New York.
[13] M. Stanoiu *et al.*, Phys. Rev. C **69**, 34312 (2004).
[14] M. Wiedeking *et al.*, Phys. Rev. C **94**, 132501 (2005).
[15] E. K. Warburton, Phys. Rev. C **38**, 935 (1988).
[16] B. A. Brown, Private communication (2004).
[17] B. M. Sherrill, D. J. Morrissey, J. A. Nolen, and J. A. Wigner, Nucl. Instrum. Methods Phys. Res. **B56**, 1106 (1991).
[18] R. Harkewicz, D. J. Morrissey, B. A. Brown, J. A. Nolen, N. Orr, B. M. Sherrill, J. S. Winfield, and J. A. Winger, Phys. Rev. C **44**, 2365 (1991).
[19] D. J. Morrissey, K. N. McDonald, D. Bazin, B. A. Brown, R. Harkewicz, N. A. Orr, B. M. Sherrill, G. A. Souliotis, M. Steiner, J. A. Wigner, et al., Nucl. Phys. A **627**, 222 (1997).
[20] A. Buta *et al.*, Nucl. Instrum. Methods Phys. Res.A **455**, 412 (2000).
[21] H. Bateman, Proc. Cambridge Philos. Soc. **15**, 423 (1910).
[22] J. C. Cooper and B. Crasemann, Phys. Rev. C **2**, 451 (1970).
[23] J. L. Wiza and R. Middleton, Phys. Rev. **143**, 676 (1966).
[24] D. J. Crozier *et al.*, Phys. Rev. C **11**, 393 (1975).
[25] N. B. Gove and M. J. Martin, Nucl. Data Tables **10**, 205 (1971).
[26] K. W. Scheller, J. Gorres, S. Vouzoukas, M. Wiescher, B. Pfeiffer, K.-L. Kratz, D. J. Morrissey, B. M. Sherrill, M. Steiner, M. Hellstrom, et al., Nucl. Phys. A **582**, 109 (1995).
[27] D. E. Alburger *et al.*, Phys. Rev. C **35**, 1479 (1987).
[28] E. Tryggestad *et al.*, Phys. Rev. C **67**, 064309 (2003).